Improved Blood Vessels Segmentation of Retinal Image of Infants

Vijay Kumar[1], Het Patel[1], Kolin Paul[1], Abhidnya Surve[2], Shorya Azad[2] and Rohan Chawla[2]
[1]*Khosla School of Information Technology, Indian Institute of Technology, Delhi, India*
[2]*Dr. Rajendra Prasad Centre for Ophthalmic Sciences, All India Institute of Medical Sciences, Delhi, India*

Keywords: Fundus Image, Retinopathy of Prematurity (ROP), Computer Aided Diagnosis (CAD), Generative Adversarial Network (GAN), U-Net, Blood Vessels Segmentation, Deep Convolutional Neural Network (DCNN).

Abstract: Retinopathy of prematurity (ROP) is the leading cause of blindness in premature babies worldwide. ROP is quantified through the structural information of the retinal vessel map, such as vessels width, tortuosity and extent. Therefore, the accuracy of quantitative studies depends on the quality of the segmented blood vessels' map. Fundus images used for neonatal eye examination are prone to many artefacts and noises due to patient movement, erratic illumination, improperly focused camera sensor, etc. Existing vessel segmentation algorithms work well on retinal images of adults but fail to detect underdeveloped vessel structures of neonatal's fundus images. At the same time, the unavailability of fundus images of infants has hindered the development of the data-driven methods for vessel segmentation. This work proposes a new Deep Convolutional Neural Network (DCNN) based vessels segmentation system for the screening for the neonatal eye disorder ROP. The proposed system uses a DCNN, Generative Adversarial Network (GAN) Pix2Pix or U-Net for vessel segmentation. Using publicly available fundus image datasets, we used an efficient and robust training procedure for the proposed system and tested them with preterm neonatal eye images from a local hospital. Experimental results show that the proposed system allows better screening of ROP with robustness to noises and inter-class variation. It has achieved an average accuracy of 96.69% for vessels segmentation and a Dice coefficient between 0.60 and 0.64. Our system is able to achieve an accuracy of 88.23% for Zone-1 case of ROP.

1 INTRODUCTION

Retinopathy of prematurity (ROP) is the leading cause of blindness in premature infants worldwide (Organization et al., 2019). ROP is caused by the abnormal development of retinal blood vessels in a preterm, light-weight infant (Gilbert et al., 2021). The International Classification of ROP (ICROP) classifies the ROP disease severity based on vascular structure, anatomical variation, and extent (Kumar et al., 2021). One such vascular activity is called Plus disease caused by changes in structural feature of blood vessels, such as vessel dilation and tortuosity (Organization et al., 2019). Analysis of retinal vessel thus holds great potential to assist the early diagnostics and treatment of the ROP and Plus diseases. In addition, it is also helpful to understand the improvement and severity of the disease (Gilbert et al., 2021). Hence, analysis of retinal vessel networks provides accurate information of ROP disease conditions. During the treatment of ROP, it is essential to accurately measure the width and tortuosity of the retinal vessels by the Ophthalmologist and computer-assisted diagnosis (CAD) software to efficiently understand and decide the line of treatment (Gilbert et al., 2021; Fielder et al., 2019).

Therefore, an automated vessel segmentation technique that accurately classifies and segments vessels from the fundus image is required. However, the structure and coloration of vessels depend on the retinal imaging procedure, the surrounding condition and the subject's ocular condition, which are highly dynamic. Due to this, developing a correct and effective technique for the segmentation of vessels becomes more complex and challenging for the image processing and computer vision communities. Specially, fundus images uses for neonatal eye examination ROP and Plus disease suffer from artifacts and noise caused by patient movement, irregular illumination (underexposure), poor contrast, eye media capacities, iris reflection and misalignment of device, etc. (Fielder et al., 2019). Existing algorithms of blood vessels segmentation have shown excellent performance with adult persons' retinal images and are based on image processing, computer vision and machine learning (ML). In recent years, data driven Deep Convolu-

Kumar, V., Patel, H., Paul, K., Surve, A., Azad, S. and Chawla, R.
Improved Blood Vessels Segmentation of Retinal Image of Infants.
DOI: 10.5220/0010849800003123
In *Proceedings of the 15th International Joint Conference on Biomedical Engineering Systems and Technologies (BIOSTEC 2022) - Volume 5: HEALTHINF*, pages 142-153
ISBN: 978-989-758-552-4; ISSN: 2184-4305

tional Neural Networks (DCNN) improve the performance of various computer vision task, such as object detection, classification, segmentation, and tracking significantly even surpass the human experts ability in many datasets (Gilbert et al., 2021). DCNN models such as Generative Adversarial Networks (GAN), U-Net or its variant have significantly high accuracy with the publicly available datasets of young person for vessels segmentation task (Wang et al., 2021; Guo et al., 2020b). These approaches, on the other hand, are unable to distinguish and identify the small, weak, and dilated branches of blood arteries. The vessels in a premature newborn's retina are smaller, thinner, and dilated, and the retina is not fully matured. Current methods for detecting and segmenting the blood vessels of a newborn's retina are ineffective. Deep learning (DL) models are also data-driven techniques that necessitate a large quantity of data for training, testing, and validation. There are no large public retinal imaging datasets available for the preterm newborn.

This study presents a DL-based technique for segmenting retinal vessels during ROP examination using the existing DCNN models, GAN and U-Net. These models are trained and fine-tuned using publically available image datasets of individuals with diabetic retinopathy (DR), glaucoma, and age-related macular degeneration (AMD). The trained model is tested on manually annotated neonatal retinal images obtained from a hospital. Furthermore, for better diagnostic accuracy, our DL-based segmentation technique for ROP screening can be applied in works such as (Kumar et al., 2021) for vascular segmentation.

The rest of the paper is organized as follows. Section 2 presents the recent work related to blood vessels segmentation. Section 3 gives the design details of the proposed DL-based method for vessels segmentation. Section 4 presents results, which comes at different stages of the proposed technique's pipeline. Finally, Section 5 summaries the proposed technique's shortcomings and future works.

2 RELATED WORK

Over the past several years, ophthalmologists have been using retinal vessels to investigate and classify retinal diseases. In this, the ophthalmologist examines the symptoms to image retinal vessels related to the disease. For its investigation, two types of methods are used. One of them is manual screening. This process is a highly biased and stressful exercise.

To overcome these limitations, ophthalmologists and researchers have chosen CAD techniques in their practice for medical diagnostic applications to detect and track vessel structure. The CAD-based techniques use image processing, computer vision, and machine learning-based algorithms to analyze retinal vessels and diagnose associated eye diseases. The CAD-based methodologies are classified into two sub-groups, one is a rule-based CAD system, and another one is data-driven CAD system techniques. The rule-based systems applications have been developed for the standard protocols and procedures that are being formulated by the experts mainly deals with vessel enhancement and segmentation. As mentioned in previous article, some popular rule-based techniques are model-based adaptive thresholding, enhance chain coding, active contours, matched filter responses, morphological operation, entropy filtering, Gabor wavelet transform, and so on (Megrabov et al., ; Kumar et al., 2021; Krestanova et al., 2020; Kubicek et al., 2019). Minor modifications or updates to the CAD system that must be updated from scratch, on the other hand, are manual and complex in rule-based screening techniques. Several data-driven techniques for medical applications have been developed in the past few years, particularly for identifying, segmenting, and monitoring retinal blood vessels. Machine learning (ML) and deep learning (DL) are data-driven algorithms that excel at image segmentation, object detection, and tracking in many medical applications. Recently, researchers have developed many vessel extraction techniques based on DCNN, which are presented in Table 1. These vessel segmentation approaches perform well on publicly available datasets of young people's retinal scans but not on infant retinal images. As shown in Figure 1, the retinal blood vessel structure does not grow properly in the preterm infant fundus image. As a result, the blood vessels of the preterm neonatal retina are blurred, and traditional vessel segmentation methods that work well with publicly available retinal image datasets do not

Table 1: Works related to blood vessel segmentation of retinal images using DNN.

Method	Dataset(Acc)	Author
RV-GAN	DRIVE (0.9790), CHASE_DB1 (0.9914), STARE (0.9887)	(Kamran et al., 2021)
U-Net	DRIVE (0.9712)	(Uysal et al., 2021)
SA-UNet	DRIVE (0.9698), CHASE_DB1 (0.9905)	(Guo et al., 2020a)
IterNet	DRIVE (0.9816), CHASE_DB1 (0.9851)	(Li et al., 2020)

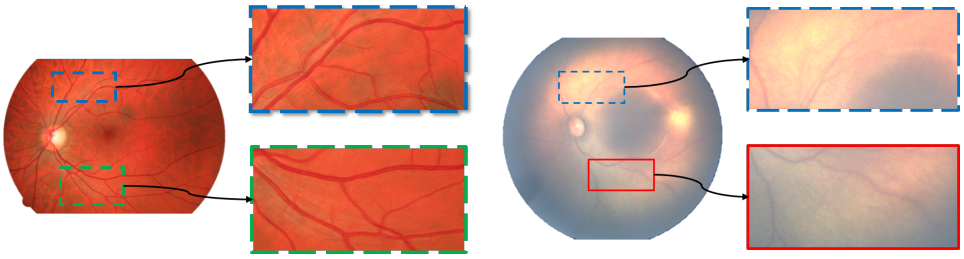

(a) Normal fundus image. (b) Neonatal fundus image.

Figure 1: Analysis of retinal vessels segmentation problem. (a) Retinal images of elderly person and the enlarge patches. (b) Neonatal fundus image and the enlarge patches.

work with the infant's retinal images.

Recently, (Yildiz et al., 2020; Luo et al., 2020) developed DCNN-based vessel segmentation techniques to segment the preterm infant retinal vessels map accurately. Here the authors used the DCNN model U-Net to segment vessels, which segment the exact vessels map of the retina image of the premature infants. The training dataset for the DL model must be carefully chosen because it affects the system's performance. These DL systems include training datasets from specific populations influenced by gender, race, age, and other factors.

To address the above problems, we have proposed a DL-based system for vessels extraction, which can operate in an environment where large-scale historical datasets are unavailable, and the accuracy of the results is highly essential. The proposed system architecture is shown in Figure 2. It mainly consists of three sections named image preprocessing, DCNN model training and testing.

3 PROPOSED APPROACH

The detailed architecture of the proposed system is shown in Figure 2. It consists of four functional units:

- Fundus imaging (or retinal scanning) unit.
- Image pre-processing.
- Blood vessels segmentation.
- Post-processing.

The Fundus Imaging Unit is responsible for taking and handling retinal scan images or videos used for retinal disease diagnosis and screening information. Ophthalmologists use a fundus camera to examine a young person's retina. However, the RitCam-3 shutter (Clarity MSI, Pleasanton, CA, USA) wide-field imaging fundus camera is used for ROP screening. A fundus image is a color image of the retinal membrane of the eye taken with a fundus camera that ophthalmologists use to diagnose and screen eye diseases. Scanned images or video data are noisy and prone to multiple errors due to uneven illumination, motion blur and sharp and sudden changes in the signal. Therefore, there is a need to improve the quality of these images. The second functional unit is the preprocessing unit, which uses image reconstruction and enhancement algorithms to reduce the impact of noise and improve image quality.

The third functional unit processes the preprocessed image using a DL-based model to segment the vessels map from the fundus image. In this study, we have considered two state-of-the-art pre-trained DL models: U-NET and GAN for the segmentation task. U-Net widely uses for image segmentation applications in the medical field. GAN is a machine learning framework inspired by game theory, in which two models, a generator and a discriminator, are competing with each other simultaneously, making each other more effective. The DL model is trained with a publicly available fundus image dataset listed in Table 2 and then used for blood vessel segmentation of neonatal fundus images.

After that, the fourth functional unit is the post-processing stage, which uses image processing and computer vision-based algorithms to extract disease-related features of the retina such as vessel width, tourist, extent, etc., from the segmented vessel map. The results exhibiting the usability of the proposed approach for Zone-1 ROP screening are discussed in Section 4.6.

3.1 Data Preparation

In this study, we have used a public dataset with a labelled blood vessels map for training and testing of both DL-models (i.e., GAN and U-net). In the validation stage, we have used the local ROP dataset of neonatal retinal images (Kumar et al., 2021). These images are raw, noisy and their pre-labelled vessel masks are also not available. However, verification of its performance requires a ground truth or gold standard. Therefore, we manually labelled preterm in-

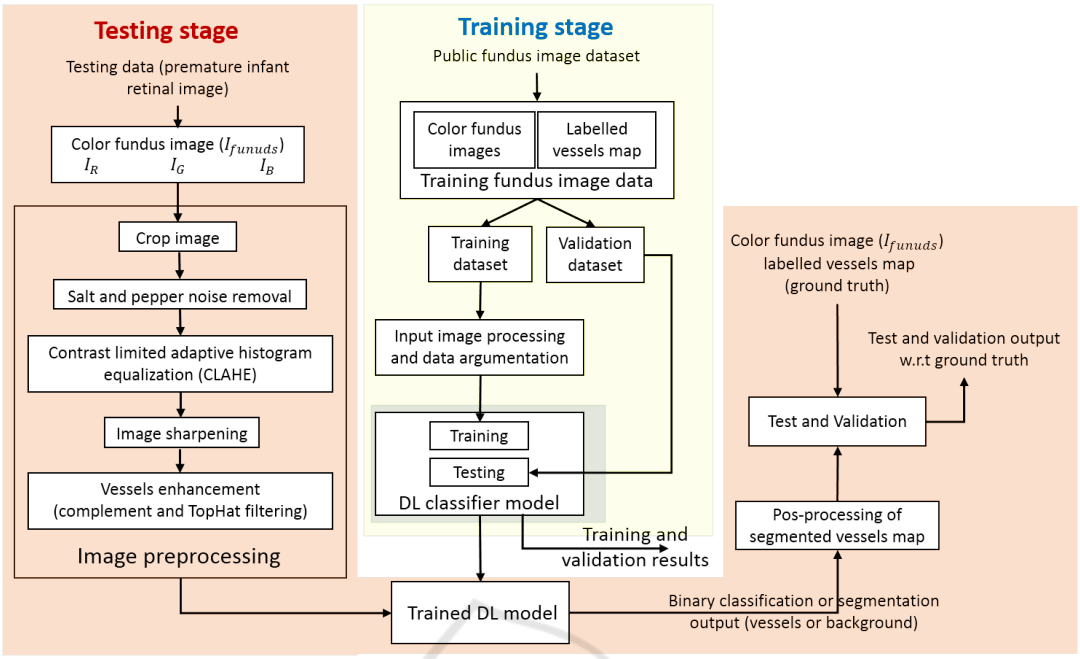

Figure 2: Block diagram representation of the full flow of Deep Learning based vessels segmentation.

fant retinal image's blood vessels to create the vessel mask. The labelling process is time consuming and laborious method. Hence, we have labelled only six image's blood vessels.

For the vessel extraction module output label, i.e. vessel map is required and generating these labels manually for the local dataset is not feasible, so the dataset for this task with the publicly available dataset with vessel maps available was collected and trained a DL based model which can generalize to the images from local dataset. Details of the compiled datasets are shown in Table 2

3.1.1 Data Pre-processing and Noise Modeling

Now to train DL based models for vessel segmentation like GAN and U-Net, the dataset mentioned in Table 2 was used. The key challenge in this is that the training dataset and test dataset is very different in terms of image quality and nature of vessels in the image as the collected images for training is from standard datasets, which contains images with very high contrast for the vessels. So in order to make these models work on ROP images, training of these models should be carried out such that they can generalize well for the noise and low contrast images as well.

So in order to make this model work, there needs to be some work done to replicate the noise and artefacts in the local dataset's image in the standard training dataset. So a noise modelling approach is proposed in which noise is added to the input image and also done some other preprocessing steps to make the training dataset(i.e. compiled dataset) more similar to the test dataset (i.e. local dataset). Table 3 summarises different functions used in noise modelling. The flowchart of the noise modelling is shown in Figure 3. Results of this noise modelling based approach can be visualized in Figure 4.

Table 2: Dataset for Vessel Segmentation.

Dataset Name	**Number of Images**
ARIA(Bankhead et al., 2012)	143
DRHAGIS(Holm et al., 2017)	40
DRIVE(Staal et al., 2004)	20
HRF(Budai et al., 2013)	45
STARE(Hoover et al., 2000)	20
Total	**288**

3.1.2 Data Augmentation by Mosaic Generation

One more experiment was carried out to increase the train dataset size by generating a synthetic dataset from the existing 288 images from the standard dataset. This synthetic dataset has been generated by following these steps. This experiment was carried out because the vessel segmentation task does not require that much global information, and also even if it would require then also normal DCNN layers employed by the proposed model is not efficient in conveying information over longer spatial distances, or

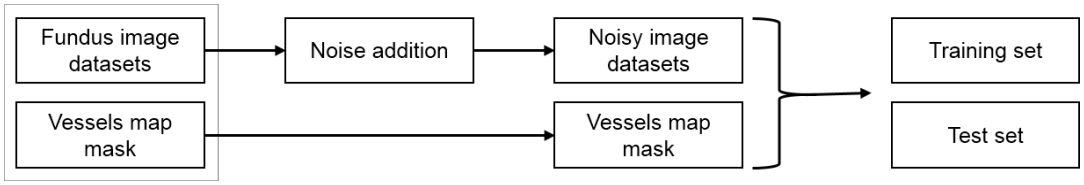

Figure 3: Training data preparation steps using noise modeling.

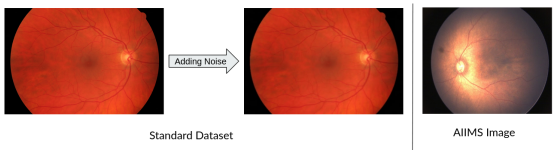

Figure 4: Results of Noise modeling and comparison with local dataset.

Table 3: Noise modeling functions.

Noise modeling	Description
crop	Image resize to 512x512
CLAHE or CLAHE(3.5, (5,5))	Contrast Limited Adaptive Histogram Equalization (CLAHE) operation with ClipLimit 3.5 and tileGridSize is (5,5).
medianBlur(3)	Median blur operation with Kernel size is 3
noise or GaussinaNoise((5,5),0)	Gaussian smoothing function with Kernek size (5,5) and standard deviation is Zero.

one can use dilated convolution layers which would require a much deeper network. So as in vessel segmentation, the model is mostly working with local information, so such augmentation methods can be useful to increase our training sample size, which can result in a better-generalized model.

1. Resize image and vessel mask to 1024x1024.
2. Break each image into 128x128 size smaller grids which will create a pool of 18432 smaller partial images.
3. Then takes 64 random samples to create one 1024x1024 mosaic image and create 500 such images to create a training dataset.

A sample image and its corresponding vessel map used while training with this augmented dataset is shown in Figure 5.

3.2 Image Pre-processing

The retinal images collected by the ophthalmologist during the retinal examination of premature infants are in a raw format and suffer from various noises, such as motion blur, irregular illumination, sudden

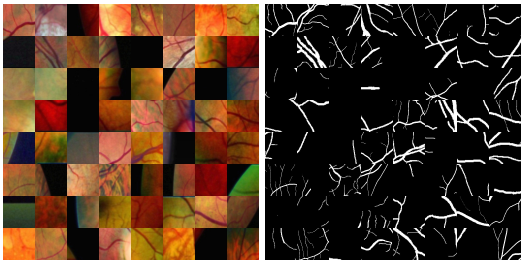

(a) Input Image. (b) Vessel Map.

Figure 5: Sample image from augmented dataset.

disturbances in image signals, etc. Noise affected images may reduce the accuracy of the proposed system result. Therefore, the image quality needs to be enhanced before these images can be used for disease detection. Preprocessing an image makes the retinal blood vessels better viewable for subsequent segmentation.

A color fundus image of a premature infant (shown in the Figure 1) is pale yellow with a map of blurred blood vessels, in which blood vessels cannot be easily seen with the naked eye. A color image frame has three color channels: red (R), green (G) and blue (B). The R-channel is saturated, while the B-channel is underexposed. Because of this, the difference between the luminance of blood vessels and the background in the R and B channel's image is indistinguishable. In G-channel, these features are clear and distinguishable for biomedical applications. Therefore, we preferred the G-channel (or gray image) and used it in further imaging experiments. We also used a mean filter and CLAHE to improve color image quality to reduce the effects of uneven illumination and motion blur.

3.3 Vessels Segmentation

Retinal blood vessels are the essential ocular system that supplies oxygen-rich blood to the cells of the retina. The small dysfunctioning, blockage or leakage of retinal blood supply to retinal cells cause ocular disorders because essential oxygen in that section of the retina is not reached. To understand and diagnose the effect ophthalmologist often uses the retinal vascular structure in diseases such as diabetic retinopa-

thy, hypertension, AMD and ROP. Especially for ROP and Plus diseases, ICROP classifies the disease extent and severity based on the retinal vessels characteristics such as tortuosity, width, extent, branches and branches angles (Gilbert et al., 2021; Kumar et al., 2021). Precise measurement of vessel characteristics by ophthalmologists or CAD software decides the effectiveness of diagnosing and investigating ROP and Plus disease (Ataer-Cansizoglu et al., 2015).

Deep learning is a technique in which a DCNN network is trained through historical pathological information related to various diseases. In the following section, we have introduced two state-of-the-art DCNNs for vessel segmentation: U-Net and GAN, which we have used in the proposed system.

3.3.1 U-Net

The architecture of the U-Net model is shown in Figure 6; it is similar to an encoder-decoder network. This network works well with biomedical segmentation as this model was designed such that it provides quality segmentation results with few training examples. The authors of (Ronneberger et al., 2015) have achieved this by proposing to replace pooling operators with up-sampling layers, due to which the model has a large number of feature channels, which allow the network to propagate context information to higher resolution layers. This model uses the simple pixel-wise soft-max $p_k(x) = exp(a_k(x))/(\Sigma_{k'=1}^{K} exp(a_{k'}(x))$ loss combined with cross-entropy loss E. For more detailed architecture, refer to the paper (Ronneberger et al., 2015).

$$E = \sum_{x \varepsilon \Omega} w(x) log(p_{l(x)}(x)) \quad (1)$$

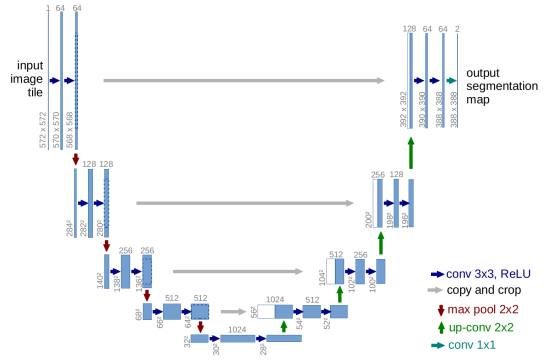

Figure 6: Architecture of U-Net (Ronneberger et al., 2015).

3.3.2 Pix2Pix GAN Model

A conditional GAN based model called Pix2Pix model developed by (Isola et al., 2018) in 2016,

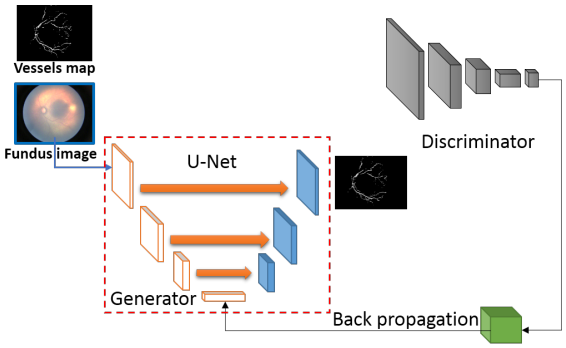

Figure 7: Pix2Pix GAN architecture in training phase.

which uses U-Net based model as a generator and another CNN model as a discriminator in the GAN training process (shown in Figure 7). These conditional GAN based models work in a way that discriminator D learns to classify between fake (synthesized by the generator) and real input_image, vessel_map tuples and Generator G learns to fool the discriminator. The Objective function to train the GAN is made up of two parts, Conditional GAN loss $\mathcal{L}_{C_{GAN}}$ and traditional L1 loss $\mathcal{L}_{L_1}$ which are mentioned in the equation below.

$$\mathcal{L}_{C_{GAN}}(G,D) = \mathbb{E}_{x,y}[logD(x,y)] + \mathbb{E}_{x,z}[log(1 - D(x,D(x,z)))] \quad (2)$$

$$\mathcal{L}_{L_1}(G) = \mathbb{E}_{x,y,z}[\|y - G(x,z)\|_1] \quad (3)$$

And final objective function is combination of both of these.

$$G^* = arg \min_G \max_D \mathcal{L}_{C_{GAN}}(G,D) + \lambda \mathcal{L}_{L_1}(G) \quad (4)$$

4 RESULTS

The proposed system and its different modules are implemented and tested on a workstation with Intel(R) Xeon(R) 40-Core CPU E5-2630 v4 @ 2.20GHz with 64 GB RAM and 8 GB NVIDIA GeForce GTX 1070 GPU.

In this section, we discuss the usability of the proposed method of vessels segmentation for the infants retinal color image capture through the RetCam. The section uses qualitative as well as quantitative methods to prove the significance of the proposed methods.

4.1 Evaluation Metrics

We have used the following evaluation metrics to evaluate the quality of the segmented blood vessels map:

1. **Accuracy:** The accuracy of the segmented result is the percentage of pixels correctly classified as True. The given equation calculates accuracy:

$$Accuracy = \frac{(TP+TN)}{(TP+TN+FP+FN)} \quad (5)$$

Where TP: True Positive, TN: True Negative, FP: False Positive and FN: False Negative are calculated to measure the effect of the classifier during pixel classification as foreground or background.

2. **Root Mean Square Error (RMSE):** This metric used the non-binary images generated by the model before the binary threshold is applied, and this finds the root of the mean squared error in these probabilities. This metric helps us find out how confident our model is. RMSE is calculated by given equation:

$$RMSE = \sqrt{\frac{1}{N}\sum_{i=1}^{N}(y_i - \hat{y}_i)^2} \quad (6)$$

Where, $\sum$ = summation ("add up"), y_i = actual image pixel, $\hat{y}_i$ = predicted image pixel and N = total number of image pixels.

3. **Peek Signal to Noise Ratio (PSNR):** This function is used mainly in signal processing and it correlates to the RMSE. Formulae for PSNR is as follows.

$$PSNR = 20log_{10}(MAX_I) - 10log_{10}(MSE) \quad (7)$$

where, MSE = Mean Squared Error = $(RMSE)^2$ and MAX_I = 255, as image pixel has max value of 255.

4. **Structural Similarity Index (SSIM):** The SSIM index is a method for measuring the similarity between two images. The SSIM index can be viewed as a quality measure of one of the images being compared, provided the other image is regarded as of perfect quality. This method helps us find out the quality of the index in terms of how similar the structure is. Detailed explanation for this metric can be found in (Wang et al., 2004).

5. **Dice Coefficient:** The Dice coefficient is similarity measure used to evaluate the segmentation task. Formula for the Dice coefficient is as follows:

$$\text{Dice coefficient} = \frac{2 * \text{Area of overlap}}{\text{Total pixels combined}} \quad (8)$$

4.2 Pre-processing of Fundus Images

We select the green channel (I_g) for analysis since it contains maximum contrast between blood vessels and background. Further, in preprocessing stage, we have to use a median filter to remove the effect of impulse noises. Impulse noise can be generated by sharp and sudden changes in image signal during acquisition. The average filter is used in the next stage, which will be reduced the effect of intensity variations across the neighbouring pixels. Further, sharping and CLAHE are used to enhance the image quality, as shown in the preprocessing results in Figure 8. In the sharpening filter, we have used unsharp masking with the standard deviation of Gaussian low pass filter is 4 and strength of sharpening effect is 1.0. Contrast-limited Adaptive Histogram Equalization (CLAHE) is used to enhance the contrast of an image by transforming the values in the intensity image. Here, we have specified the number of tiles in a row, column and contrast enhance limit is 8×8 and 0.005 respectively and remaining all parameters such as the number of bins for histogram (= 256), output image intensity range (= 0 to 255), histogram distribution type (= $uniform$), and distribution parameters (= 0.4) are selected default value of MATLAB R2020b CLAHE[1] function.

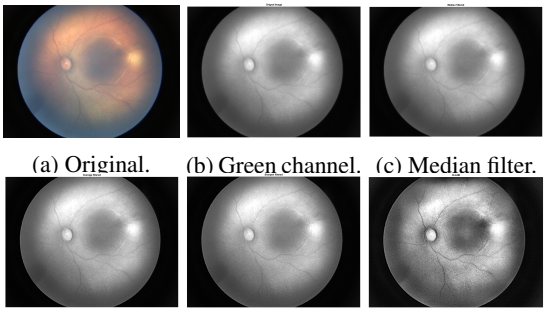

(a) Original. (b) Green channel. (c) Median filter.

(d) Average filter. (e) Sharpen. (f) Enhanced.

Figure 8: Output images of different stages of preprocessing of original color (RGB) image.

4.3 DL-Model Training and Testing

Deep learning is a technique, in which DCNN model get trained through the historical labelled images related to pathological information related to different disease. In the following section, we have discussed two state-of-art DL-based networks for vessels segmentation.

4.3.1 GAN based Approach

Now after preparing the data by noise modeling and data augmentation, a conditional-GAN based model called pix2pix (Isola et al., 2018) was trained.

[1] mathworks.com/help/images/ref/adapthisteq

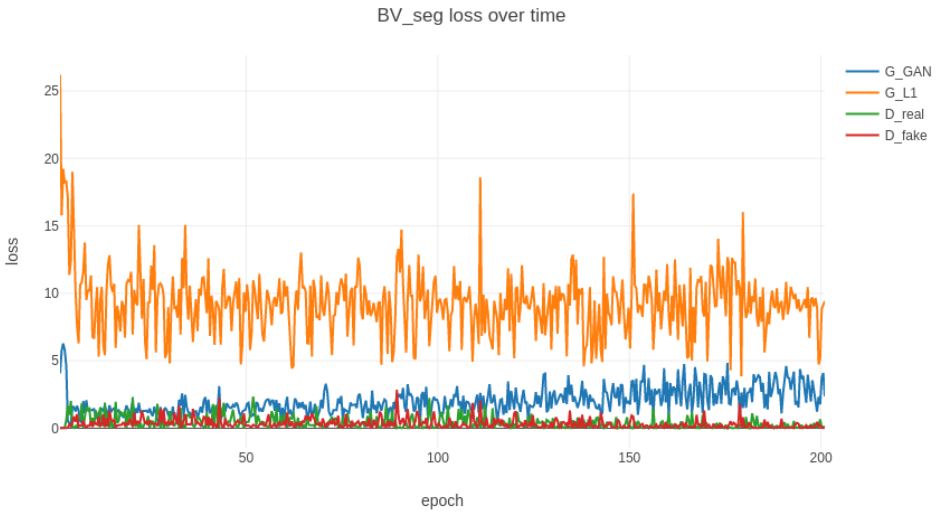

Figure 9: Training History plot for GAN model.

Now during training, the plot for generator and discriminator loss functions for each step is shown in Figure 9 for each model. In this plot, the loss value is very high due to random weight assignment, but as training progresses, it has reduced, but loss values oscillate. This is due to a general characteristic of GAN as both of them works against and for each other. The base code for the pix2pix model can be found on GitHub repository[2].

To obtain the optimal model, multiple combinations of input image size, different model parameters, data without noise modelling, data with noise modelling, augmented dataset during training and model using input image type are used during training, and the best model was found among them. More details about all these combinations are shown in Table 6.

4.3.2 U-Net based Approach

The conditional GAN based model that was discussed in the past section uses U-Net as Generator and the main difference between GAN and any other encoder-decoder based networks like U-Net is in training the network as GAN has conditional-GAN's objective function in the training process. So sometimes, this would lead to overfitting with a smaller dataset. So experiments were carried out by trying out vanilla U-Net (Ronneberger et al., 2015), without GAN loss, which was developed for the biomedical image segmentation.

So to train the U-Net model, the same dataset mentioned in Table 2 was used, and the noise modelling shown in 3.1.1 was also used on top of raw images. Augmented dataset discussed in 3.1.2 was also

[2]github.com/junyanz/pytorch-CycleGAN-and-pix2pix

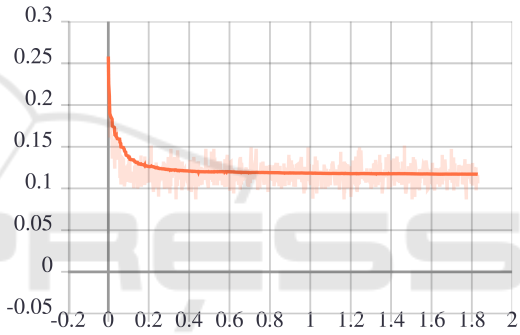

Figure 10: Loss Function v/s time for Train Dataset.

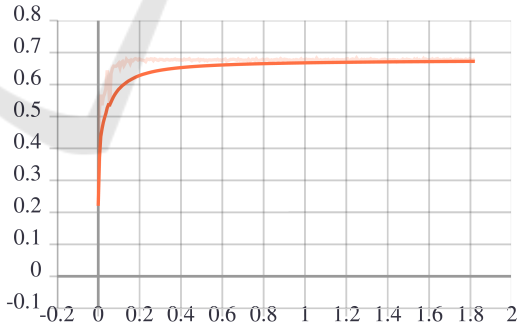

Figure 11: Dice coefficient v/s time for Validation Dataset.

used to train the U-Net model. A similar combination of models used for training the GAN model was used here also to train various U-Net models to find out the best model amongst all these combinations. All these models were trained for 100 epochs with a constant learning rate of 0.0001(Refer to Table 6 for more information).

While training the model, the plot for the best model and almost all models looked like as shown in the Figure 10 and 11, from these plots, one can infer

that dice co-efficient for the Validation dataset is increasing, which is a metric to find the performance of the segmentation model and loss function on training dataset is decreasing as training progresses. So one can say that model should generalize well in the testing, which is reflected in the results. The codebase used for U-Net can be found on GitHub repository [3].

4.4 Blood Vessels Segmentation

In this section, we evaluate the performance of the proposed system to segment the nascent corpuscle images vessels. We used accuracy, RMSE, PSNR and SSIM as performance metrics to measure the quality of the segmentation, and its high value indicates the best quality.

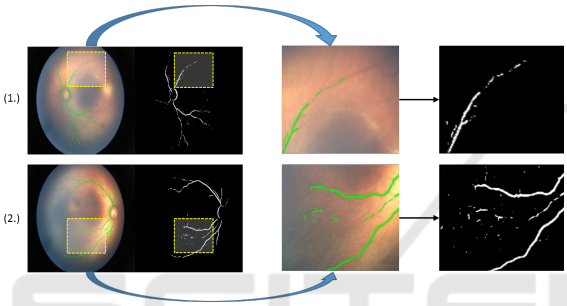

Figure 12: Retinal vessel segmentation using U-net. In image (1) and (2) patch ROI-1 and ROI-2 are used to analyze the segmented blood vessels map in detail.

Table 4: Bench-marking Results from U-Net model.

Image	Accuracy	RMSE	PSNR	SSIM
Img_1	97.56	0.15	16.82	0.93
Img_2	97.55	0.16	16.80	0.92
Img_3	92.66	0.27	11.60	0.85
Img_4	97.27	0.16	16.14	0.92
Img_5	97.46	0.15	16.70	0.93
Img_6	97.26	0.17	16.31	0.92
Mean	**96.63**	**0.18**	**15.73**	**0.91**

4.4.1 Segmentation using U-Net

Among all of the trained models, the model with the augmented dataset performed the best in the case of U-Net. Now to get the general overview of the performance of the model, the qualitative analysis was carried out for the local dataset, and this model is generating good results for our dataset (as shown in Figure 12). Quantitative analysis was also done on the few labelled examples from the local dataset as it was also done for the GAN model. Refer to Table 4 for the results. This table reflects that this model is performing well for the image with noise and over-exposed shots where vessels are not well separated from the background, and also the performance figures are also very much similar to what the GAN model has produced, but this model is much simpler compared to GAN model in terms of training as well as detection.

[3] github.com/milesial/Pytorch-UNet

4.4.2 Segmentation using GAN

Now for the evaluation of the vessel extraction model, qualitative methods were employed, which required manual inspection of all the results generated by the model for the local dataset. The models trained by noise modelling gave good results, although models trained with augmented dataset displayed some edge like artefacts in the test images due to the nature of mosaic images used in training, this dataset will be used afterwards, and it has shown promising results for other models. The result from the GAN model is shown in the Figure 13.

Table 5 summarized the vessels segmentation results with preterm retinal images from local ROP distastes. In which, we have reported proposed segmentation techniques' result when trainable DL-model is used for vessels segmentation. Statistically, the evaluation metrics such as Accuracy, RMSE, PSNR and SSIM score is high and comparable with respect to the U-net network. However, for the GAN model,

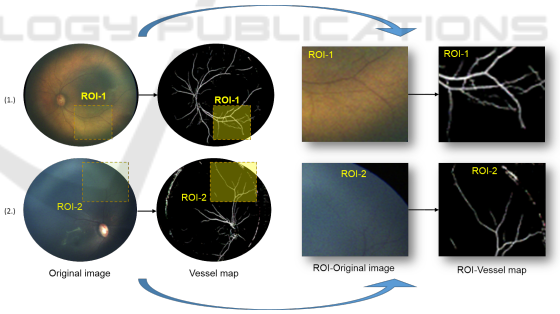

Figure 13: Retinal vessel segmentation using GAN on local dataset. In image, (1) and (2) patch ROI-1 and ROI-2 are used to analyze the segmented blood vessels map in detail.

Table 5: Bench-marking Results from GAN(pix2pix) model.

Image	Accuracy	RMSE	PSNR	SSIM
Img_1	97.51	0.16	16.89	0.89
Img_2	97.76	0.15	16.14	0.91
Img_3	92.80	0.27	11.70	0.81
Img_4	97.62	0.15	17.15	0.90
Img_5	97.30	0.16	16.74	0.89
Img_6	97.15	0.17	16.29	0.88
Mean	**96.69**	**0.18**	**16.15**	**0.88**

Table 6: Different combinations of models trained for U-net/GAN.

Model_name	Pre-processing steps	Color	Resolution	Dice-coeff.
orig	crop	rgb	512x512	0.42-0.44
noise	crop+GaussianNoise((9,9),0)	rgb	512x512	0.38-0.42
noise+clahe	noise+clahe(3.5,(5,5))+medianBlur(3)	rgb	512x512	0.58-0.6
orig_bw	crop	gray	512x512	0.58-0.59
noise_bw	crop+GaussianNoise((5,5),0)	gray	512x512	0.52-0.53
noise+clahe_bw	noise+clahe(3.5,(5,5))+medianBlur(3)	gray	512x512	0.59-0.60
noise_bw	crop+GaussianNoise((9,9),0)	gray	512x512	0.54-0.55
noise+clahe_bw	noise+clahe(3.5,(5,5))+medianBlur(3)	gray	512x512	0.55-0.56
noise+clahe_bw+bicubic_upscal	noise+clahe(3.5,(5,5))+medianBlur(3)	gray	512x512	0.60-0.64
noise+clahe+bicubic_upscal	noise+clahe(3.5,(5,5))+medianBlur(3)	rgb	512x512	0.57-0.59
noise+clahe_bw+bicubic_upscal	noise+clahe(3.5,(5,5))+medianBlur(3)	gray	256x256	0.60-0.62
noise+clahe+bicubic_upscal	noise+clahe(3.5,(5,5))+medianBlur(3)	rgb	256x256	0.59-0.60
noise+clahe_bw+bicubic_upscal	noise+clahe(3.5,(5,5))+medianBlur(3)	gray	1024x1024	0.61-0.62
noise+clahe+bicubic_upscal	noise+clahe(3.5,(5,5))+medianBlur(3)	rgb	1024x1024	0.48-0.50

we achieve an average accuracy of 96.69% is sightly higher than the accuracy value of the U-Net model 96.63.

4.5 Various Combinations for Vessel Extraction Models

Now in order to get the model for the vessel extraction, multiple experiments were carried out by changing various fields, and while training these models, due to the lack of ground truth for the local dataset, the validation using any kind of performance metric for segmentation was not carried out. So many experiments were carried out, tweaking multiple parameters and after doing qualitative analysis of the generated results, carried out the next experiments.

- **Noise Modeling:** Proposed noise modelling based approach in 3.1.1 during for training dataset to bridge the gap between training and test dataset as they have a very distinct characteristic.
- **Pre-Processing:** This is applied to test as well as training examples to enhance the contrast using the CLAHE Filter.
- **Color Channels:** Noticed during the initial phase of experiments that models with only single-channel (i.e., G-channel) gray-scale images can give better results for vessel segmentation so, for some combinations, both RGB and gray-scale images were used as input.
- **Resolution:** This was a major part of the given model as it decided the time taken to train and extract the blood vessels from the image as it can change the size of the model.
- **Grid Size for Augmented Dataset:** Tried out multiple grid sizes for the dataset that was augmented as mentioned in 3.1.2.
- **Upscaling Algorithm:** Both models use U-Net either directly or indirectly, and de-convolution is part of it, and upscaling can be done in two ways, either bilinear upscaling or bicubic upscaling (Ronneberger et al., 2015). By default, U-Net uses Bilinear upscaling as it has a lower computational cost, but some experiments have also tried out bicubic upscaling algorithm as it is known to give better results, but it results in higher computational time.

Now all the combinations that were tried out with specific pre-processing steps are listed in Table 6 for the original dataset(i.e. without image mosaic based augmentation). Keep in mind that in all these experiments training dataset is of size 224, and the model was trained for 100 epochs with a learning rate of 0.0001.

The models trained using the augmented dataset from Section 3.1.2 using mosaic is listed in Table 7 and in all these experiments training dataset has 450 samples and models were trained for 100 epochs with a 0.0001 learning rate.

Without noise modelling and preprocessing, the U-Net and GAN model gives dice coefficient between 0.42-0.44 for vessels segmentation with the local dataset. However, for the same network and task (Kamran et al., 2021; Uysal et al., 2021; Guo et al., 2020a; Li et al., 2020), reported dice coefficient more than 0.70 with publicly available dataset such as DRIVE STARE or CHASE_DB1. However, using the proposed system, we get significant improvement in the Dice Coefficient and accuracy of vessels seg-

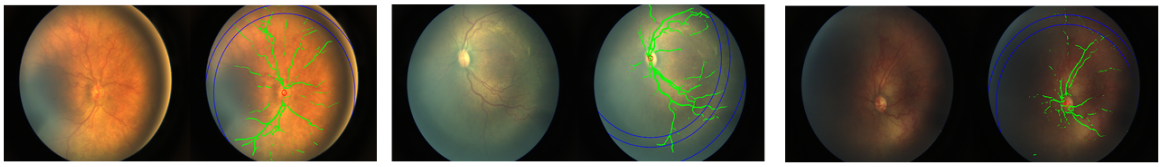

Figure 14: Visualization of Zoning algorithm.

Table 7: Different Combinations of models trained for U-Net/GAN with dataset augmented using mosaic generation in input image of size 512x512 pixels and its Dice coefficient in the last step.

Model_name	**rgb/gray**	**Dice-coeff.**	**Grid Size**
noise+ clahe_bw+ bicubic upscaling	gray	0.678-0.68	32x32
noise+ clahe+ bicubic upscaling	rgb	0.685+	32x32
noise+ clahe_bw+ bicubic upscaling	gray	0.67-0.68	64x64
noise+ clahe+ bicubic upscaling	rgb	0.67+	64x64

mentation with the ROP dataset. At the same time, its performance got reduced for the public datasets, as we have used preprocessed (or noise modelling) images.

4.6 Zone-1 ROP Screening

Our next set of experiments showed that the GANs based vessel detection had better generalization in terms of quality of vessel maps generated and detect thinner vessels on the posterior regions of the fundus image helping in the zoning algorithm (ICROP) (Kumar et al., 2021). Zoning algorithm gave the accuracy of **88.23%** on the local dataset. The image 14 shows detection of the extent of vessel growth pretty accurately even in case of some tricky images with noise or high exposure or even in case of very dark images, using GANs based vessel detection.

5 CONCLUSION AND DISCUSSION

Precise segmentation and detection of blood vessels is an essential task for efficiently diagnosing and monitoring ROP and Plus disease in neonatal-ophthalmology. In this paper, we propose a new retinal vessel segmentation method using the DCNN architectures, in which retinal scans are indistinguishable from image/video noise, blur, and vessels map background. We have used two existing Pix2Pix of U-Net and GAN model for same. The proposed method of dataset preparation are used to trained and tested on publicly available datasets and evaluated its performance on the ROP dataset. The proposed system achieves a high Dice coefficient and accuracy rate for the retinal vessel segmentation task.

In addition, we tested our approach on retinal scans of premature newborns at a nearby hospital. Our approach significantly improves the Zoning based ROP classification as it is based on the extent of blood vessels. However, for the Plus disease requires structural information of the vessel such as tortuosity, branch angle and width. The proposed work provides greater interest in utilising deep learning-based systems in the future to develop similar applications such as disease screening, diagnosis and monitoring using biomedical (retinal) images. The proposed system can be specially used to develop automated applications for fundus imaging-based affordable health care in the future (Moshfeghi and Capone, 2018; Kumar and Paul, 2016; Paul and Kumar, 2015; Patel et al., 2019). Therefore, this will require a research study that we expect to significantly improve using the new DL-based vessel segmentation technique in resource-constraint environments.

REFERENCES

Ataer-Cansizoglu, E., Bolon-Canedo, V., Campbell, J. P., Bozkurt, A., Erdogmus, D., Kalpathy-Cramer, J., Patel, S., Jonas, K., Chan, R. P., Ostmo, S., et al. (2015). Computer-based image analysis for plus disease diagnosis in retinopathy of prematurity: performance of the "i-rop" system and image features associated with expert diagnosis. *Translational vision science & technology*, 4(6):5–5.

Bankhead, P., Scholfield, C. N., McGeown, J. G., and Curtis, T. M. (2012). Fast retinal vessel detection and measurement using wavelets and edge location refinement. *PloS one*, 7(3):e32435.

Budai, A., Bock, R., Maier, A., Hornegger, J., and Michelson, G. (2013). Robust vessel segmentation in fundus images. *International journal of biomedical imaging*, 2013.

Fielder, A. R., Wallace, D. K., Stahl, A., Reynolds, J. D., Chiang, M. F., and Quinn, G. E. (2019). Describing retinopathy of prematurity: Current limitations and new challenges. *Ophthalmology*, 126(5):652–654.

Gilbert, C., Malik, A. N., and Vinekar, A. (2021). Artificial intelligence for rop screening and to assess quality of care: Progress and challenges. *Pediatrics*, 147(3).

Guo, C., Szemenyei, M., Yi, Y., Wang, W., Chen, B., and Fan, C. (2020a). Sa-unet: Spatial attention u-net for retinal vessel segmentation. *arXiv preprint arXiv:2004.03696*.

Guo, X., Chen, C., Lu, Y., Meng, K., Chen, H., Zhou, K., Wang, Z., and Xiao, R. (2020b). Retinal vessel segmentation combined with generative adversarial networks and dense u-net. *IEEE Access*, 8:194551–194560.

Holm, S., Russell, G., Nourrit, V., and McLoughlin, N. (2017). Dr hagis—a fundus image database for the automatic extraction of retinal surface vessels from diabetic patients. *Journal of Medical Imaging*, 4(1):014503.

Hoover, A. D., Kouznetsova, V., and Goldbaum, M. (2000). Locating blood vessels in retinal images by piecewise threshold probing of a matched filter response. *IEEE Transactions on Medical Imaging*, 19(3):203–210.

Isola, P., Zhu, J.-Y., Zhou, T., and Efros, A. A. (2018). Image-to-image translation with conditional adversarial networks.

Kamran, S. A., Hossain, K. F., Tavakkoli, A., Zuckerbrod, S. L., Sanders, K. M., and Baker, S. A. (2021). Rv-gan: Segmenting retinal vascular structure in fundus photographs using a novel multi-scale generative adversarial network. In *International Conference on Medical Image Computing and Computer-Assisted Intervention*, pages 34–44. Springer.

Krestanova, A., Kubicek, J., Penhaker, M., and Timkovic, J. (2020). Premature infant blood vessel segmentation of retinal images based on hybrid method for the determination of tortuosity. *Lékař a technika-Clinician and Technology*, 50(2):49–57.

Kubicek, J., Timkovic, J., Penhaker, M., Oczka, D., Kovarova, V., Krestanova, A., Augustynek, M., and Cerny, M. (2019). Detection and segmentation of retinal lesions in retcam 3 images based on active contours driven by statistical local features. *Advances in Electrical and Electronic Engineering*, 17(2):194–201.

Kumar, V., Patel, H., Paul, K., Surve, A., Azad, S., and Chawla, R. (2021). Deep learning assisted retinopathy of prematurity screening technique. In *HEALTHINF*, pages 234–243.

Kumar, V. and Paul, K. (2016). mnetra: A fundoscopy based optometer. In *HEALTHINF*, pages 83–92.

Li, L., Verma, M., Nakashima, Y., Nagahara, H., and Kawasaki, R. (2020). Iternet: Retinal image segmentation utilizing structural redundancy in vessel networks. In *Proceedings of the IEEE/CVF Winter Conference on Applications of Computer Vision*, pages 3656–3665.

Luo, Y., Chen, K., Mao, J., Shen, L., and Sun, M. (2020). A fusion deep convolutional neural network based on pathological features for diagnosing plus disease in retinopathy of prematurity. *Investigative Ophthalmology & Visual Science*, 61(7):2017–2017.

Megrabov, E., Jamshidi, A., and Patange, S. Retinel vessel segmentation using u-net and gans.

Moshfeghi, D. M. and Capone, A. (2018). Economic barriers in retinopathy of prematurity management. *Ophthalmology Retina*, 2(12):1177–1178.

Organization, W. H. et al. (2019). World report on vision. Technical report, Geneva: World Health Organization.

Patel, T. P., Aaberg, M. T., Paulus, Y. M., Lieu, P., Dedania, V. S., Qian, C. X., Besirli, C. G., Margolis, T., Fletcher, D. A., and Kim, T. N. (2019). Smartphone-based fundus photography for screening of plus-disease retinopathy of prematurity. *Graefe's Archive for Clinical and Experimental Ophthalmology*, 257(11):2579–2585.

Paul, K. and Kumar, V. (2015). Fundus imaging based affordable eye care. In *HEALTHINF*, pages 634–641.

Ronneberger, O., Fischer, P., and Brox, T. (2015). U-net: Convolutional networks for biomedical image segmentation.

Staal, J., Abramoff, M., Niemeijer, M., Viergever, M., and van Ginneken, B. (2004). Ridge based vessel segmentation in color images of the retina. *IEEE Transactions on Medical Imaging*, 23(4):501–509.

Uysal, E. S., Bilici, M. Ş., Zaza, B. S., Özgenç, M. Y., and Boyar, O. (2021). Exploring the limits of data augmentation for retinal vessel segmentation. *arXiv preprint arXiv:2105.09365*.

Wang, Z., Bovik, A. C., Sheikh, H. R., and Simoncelli, E. P. (2004). Image Quality Assessment: From Error Visibility to Structural Similarity. *IEEE Transactions on Image Processing*, 13(4):600–612.

Wang, Z., She, Q., and Ward, T. E. (2021). Generative adversarial networks in computer vision: A survey and taxonomy. *ACM Computing Surveys (CSUR)*, 54(2):1–38.

Yildiz, V. M., Tian, P., Yildiz, I., Brown, J. M., Kalpathy-Cramer, J., Dy, J., Ioannidis, S., Erdogmus, D., Ostmo, S., Kim, S. J., et al. (2020). Plus disease in retinopathy of prematurity: Convolutional neural network performance using a combined neural network and feature extraction approach. *Translational Vision Science & Technology*, 9(2):10–10.